JOURNAL OF GEOPHYSICAL RESEARCH, VOL. 91, NO. C7, PAGES 8497–8508, JULY 15, 1986

Wind-Driven Surface Transport in Stratified Closed Basins: Direct Versus Residual Circulations

P. TED STRUB

College of Oceanography, Oregon State University, Corvallis

THOMAS M. POWELL

Division of Environmental Studies, University of California, Davis

A numerical model has been used to investigate the wind-driven circulation in a stratified basin of moderate size, Lake Tahoe, California-Nevada. Two types of circulation are identified: "direct" circulations, in which the current directions remain relatively constant and the mean circulation formed over several days resembles the instantaneous circulation, and "residual" circulations, in which the currents fluctuate continuously and the mean circulation is characterized by small net displacements of parcels after large oscillations. Previous studies of stratified closed basins have emphasized residual circulations caused by cyclonically propagating internal basin modes, resulting in a single cyclonic mean gyre during light to moderate winds. Observations at Lake Tahoe have shown currents which are more constant in direction, with a double gyre pattern of surface circulation, dominated by an anticyclonic northern gyre. Model experiments of Lake Tahoe demonstrate that the curl of the wind stress must be included to obtain a direct, double gyre circulation similar to the observations. Horizontally uniform winds cause a residual circulation, similar to that reported at other lakes. Use of the model to calculate the vorticity budget clarifies the role of the wind stress curl in creating the direct double gyre.

1. INTRODUCTION

In this paper we investigate the dynamics of wind-driven circulations in moderate-sized, stratified basins. The work is motivated by the contrast between observations at Lake Tahoe and past studies of the circulations of a number of other real and idealized closed basins. The dynamics apply to stratified basins of 10–100 km in horizontal dimension, where the internal Rossby radius of deformation is an order of magnitude less than the basin dimension but the basin is too small to be influenced by latitudinal variation in the Coriolis parameter. In such systems, large-scale vertical displacements of internal density surfaces are trapped near the coast by the earth's rotation and propagate cyclonically around the basin. In smaller basins these displacements propagate directly across the entire basin as internal seiches in a period much less than the inertial period. In the much larger basins of the world oceans, dissipation, changes in coastal topography, and Rossby waves propagating away from the eastern coast deplete the energy in the waves before they can travel completely around the basin.

In the basins considered here, these trapped waves travel cyclonically around the basin as Kelvin or topographic waves, and a repeated series of waves may result from repeated wind forcing, such as a diurnal wind cycle or a series of synoptic storms. The instantaneous velocities associated with the waves fluctuate, causing water parcels to move in an oscillatory fashion that results in a small net displacement after each oscillation. The net basin-wide circulation created by these waves is characterized by mean velocities (when averaged over several wave periods) that are much less than the instantaneous values. Such circulations are referred to as residual circulations [*Cheng and Casulli*, 1982]. An alternative to a residual circulation is a direct circulation, where parcels move continuously in large gyral patterns, and the mean velocities are similar in magnitude and direction to the instantaneous velocities. The literature describing the circulations of stratified idealized basins, the Great Lakes, and lakes of the 10- to 20-km size emphasizes residual circulations as causing the often observed single cyclonic gyre [*Ball*, 1965; *Ou and Bennett*, 1979; *Simons*, 1980; *Mysak et al.*, 1983].

In Lake Tahoe, mixed layer currents measured during the summer by moored current meters are relatively constant in direction, rather than fluctuating [*Dillon and Powell*, 1976, 1979]. More recently, horizontal patterns of surface circulation inferred from sequences of summer infrared (IR) satellite images are seen to consist of a double gyre, dominated by an anticyclonic northern gyre, with a weaker cyclonic southern gyre [*Strub et al.*, 1984]. Other scattered past observations, such as transport of inflowing sediments, plumes, and locations of primary productivity maxima [*Goldman*, 1974], agree with the circulation patterns inferred from the satellite IR images. Thus we ask why the circulation of Lake Tahoe differs from that of other basins?

2. BACKGROUND

Circulation in Closed Basins

In homogeneous basins, typical of lakes during winter and early spring, circulation patterns are often discussed in terms of the vertically integrated transport. A number of authors have described the horizontal patterns of transport in such basins [*Rao and Murthy*, 1970; *Csanady*, 1975; *Simons*, 1980]. In general, they find that a constant, uniform wind stress causes a topographically controlled two-gyre circulation, with downwind transport in the shallow, nearshore regions and return flow in the deeper central basin. At the surface, wind stress drives water downwind, eventually creating a surface slope and pressure gradient which opposes the wind stress.

Paper number 6C0140.
0148-0227/86/006C-0140$05.00

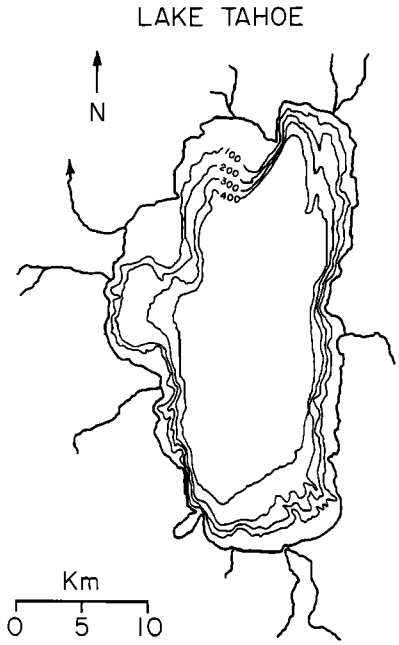

Fig. 1. Bathymetry of Lake Tahoe.

The effect of the wind stress on the water column decreases where the basin is deep, but the pressure gradient does not, causing return flow at depth, which leads to the net (vertically integrated) return flow where the water is deeper than the mean depth. The earth's rotation causes the two-gyre system to rotate cyclonically around the basin due to the conservation of potential vorticity [*Csanady*, 1975]. *Huang and Saylor* [1982] show that cyclonic rotation of the double gyre in southern Lake Michigan can produce oscillating currents with periods of approximately 90 hours, as observed by *Saylor et al.* [1980]. They argue that waves of different periods (free waves in the deeper basin and forced waves near the shore) interact to produce the 90-hour period and suggest that resonance with the wind selects this period. *Schwab* [1983] also models Lake Michigan for the homogeneous case and finds the northern and southern basins to act separately, with a pair of gyres in each. The rotation of the gyres is clearer in the south, and he finds no evidence of resonance with the wind.

In homogeneous basins driven by a horizontally varying wind field, changes in both depth and wind stress become important. The effects of horizontal variations in both wind stress and basin depth can be evaluated using the linear equation for the conservation of mean (vertically averaged) flow vorticity [*Csanady*, 1975]:

$$\frac{\partial}{\partial t}\left(\frac{\partial \bar{v}}{\partial x}-\frac{\partial \bar{u}}{\partial y}\right)=\mathbf{k}\cdot\operatorname{curl}\left(\frac{\tau}{H}\right) \tag{1}$$

where $\bar{u}$ and $\bar{v}$ are the depth-averaged velocity (similar to vertically integrated transport), τ is the surface wind stress, H is the water depth, and $\mathbf{k}$ is a unit vector in the vertical. The rate of change of mean flow vorticity, seen on the left, describes the creation of cyclonic (positive vorticity) or anticyclonic (negative vorticity) flow. In flat, homogeneous basins the curl of the wind stress will determine the gyral patterns. In a model of the relatively flat and shallow central portion of Lake Erie, forced by strong (~8–11 m/s) winds, a 3 m/s north-south difference in the eastward wind stress causes the dominance of either the northern anticylonic or the southern cyclonic gyre, depending on whether the wind is greater in the north or south (D. Schwab, personal communication, 1986). If both τ and H are variable in space, the right-hand side of (1) can be broken into two terms, and these can be used to show that variations in wind stress will dominate those of depth if, over the region considered,

$$\frac{\Delta\tau}{\tau}>\frac{\Delta H}{H}$$

i.e., if the relative variation in wind stress is greater than that of the basin depth over the same horizontal scale. Lake Tahoe's central basin (Figure 1) is relatively flat, and use of the above scaling shows that differences in wind speed of less than 0.5 m/s across the basin will dominate the change in depth for light (3 m/s) winds, while differences of approximately 1.0 m/s will dominate for strong (10 m/s) winds. This suggests that the winter and early spring response of Lake Tahoe should be sensitive to the wind stress curl. This also applies to the barotropic component of the flow under stratified conditions.

In stratified basins, typical of summer and early autumn conditions, studies of the wind-driven currents emphasize that baroclinic motions, rather than bottom topography, determine the long-term circulation patterns [*Simons*, 1980]. For a layered fluid, as described in the appendix, the sources and sinks of vorticity in the surface layer are found by cross differentiating the linear equations for transport in the layer (A2), resulting in the linear, baroclinic, transport vorticity equation:

$$\frac{\partial\zeta}{\partial t}=-gJ(d,\eta)-f\left[\frac{\partial U}{\partial x}+\frac{\partial V}{\partial y}\right]+\frac{1}{\rho}\mathbf{k}\cdot\operatorname{curl}(\tau)-\frac{1}{\rho}\mathbf{k}\cdot\operatorname{curl}(\tau_b)-A_h\nabla_h^2\zeta \tag{2}$$

where

$$\zeta=\frac{\partial V}{\partial x}-\frac{\partial U}{\partial y}$$

is the vorticity of the layer transport, g is the acceleration of gravity, d is the thickness of the surface layer, η is the surface elevation, ϕ is the local Coriolis parameter, U and V are the vertically integrated x and y transports in the layer, ρ is the density, τ is the wind stress, τ_b is the stress at the bottom of the surface layer (either interfacial friction or bottom friction), A_h is a horizontal eddy viscosity, and

$$\nabla_h=\mathbf{i}\frac{\partial}{\partial x}+\mathbf{j}\frac{\partial}{\partial y}$$

J is the Jacobian operator,

$$J(a,b)=\frac{\partial a}{\partial x}\frac{\partial b}{\partial y}-\frac{\partial b}{\partial x}\frac{\partial a}{\partial y}$$

The vertically integrated pressure gradient has been expressed as $-g\,d\,\nabla_h\eta$.

The generation of cyclonic or anticyclonic vorticity depends on the balance of the five terms on the right of (2). The first term on the right of (2) describes the generation of vorticity by pressure forces caused by internal surfaces slanting at different angles for different levels, an entirely baroclinic contribution. The second term on the right represents the conversion of planetary to local vorticity by vortex stretching, as represented by the divergence. In a homogeneous, barotropic fluid, bottom topography is the source of this divergence, whereas in a stratified, baroclinic fluid, internal motions are the primary source of divergence in the surface layer. Thus the first two terms are

largely the result of internal motions of layer surfaces. The third and fourth terms are the direct fluxes of vorticity across the top and bottom boundaries of the layer caused by the curl of the wind stress and friction, respectively. In a layered basin driven from above, one normally thinks of the surface wind stress curl as a source and the bottom friction curl as a sink of vorticity in the top layer. The fifth term represents horizontal diffusion of vorticity and must be a sink overall. Thus baroclinic motion (i.e., the pressure and divergence terms) and curl of the surface wind stress are sources of vorticity, while curl of the bottom stress and horizontal diffusion are sinks of vorticity in the surface layer.

In a model of Lake Ontario's July circulation, *Huang and Sloss* [1981] found that the baroclinic terms contributed to cyclonic vorticity, resulting in a monthly averaged single cyclonic surface gyre. The circulation agrees with observations by *Pickett and Richards* [1975]. The model was driven by measured winds which were usually light and from the west. Although no horizontal variation in the wind field was allowed, a cyclonic curl in the wind stress field arose through the stability dependent drag coefficient used to calculate wind stress from wind velocity. This curl contributed to the cyclonic circulation, as discussed by *Emery and Csanady*, [1973]. During several days of stronger westerly winds a two-gyre pattern developed, similar to the winter pattern, which decayed back to the single gyre when the winds relaxed. *Simons* [1975] simulated August currents in Lake Ontario following strong northwest winds and found a similar result: strong winds initially forced a two-gyre pattern, but as the winds decreased, the cyclonic southeast gyre became dominant over most of the lake. Using both analytic and numerical methods, *Ou and Bennett* [1979] found that the nonlinear resonant interaction of the diurnal wind and baroclinic Kelvin waves resulted in a residual cyclonic flow in an idealized basin the size of Lake Kinneret (similar in size to Lake Tahoe), in agreement with current measurements [*Serruya*, 1975]. No curl in the wind stress was allowed. *Bennett* [1977, 1978] has explored the mechanisms responsible for the dominance of a cyclonic gyre in idealized stratified basins. His conclusions also indicate that effects of the transient displacement of the thermocline are responsible for a cyclonic residual circulation.

In the absence of strong wind forcing, these studies suggest that the dynamics of many stratified basins are dominated by the interaction of horizontally uniform winds and baroclinic motions, which result in a single residual cyclonic gyre. Strong winds (still horizontally uniform) may produce a double gyre, cyclonic in the half of the basin to the right of the downwind direction and anticylonic in the half to the left. Few investigators have considered effects of horizontal variation in the wind field itself. The argument is usually made that the length scales of variations in the strongest winds are large (the 1000-km synoptic storm scale) compared to the basin size, and thus horizontal variation across the basin must be small. *Simons* [1985] evaluated the effect of including the wind stress curl in a linear model of Lake Ontario under homogeneous winter conditions and found only a small effect on the low-frequency model currents. The present paper differs from Simons' study in that it evaluates the effect of wind stress curl on modeled currents caused by the diurnal summer wind regime in a stratified lake.

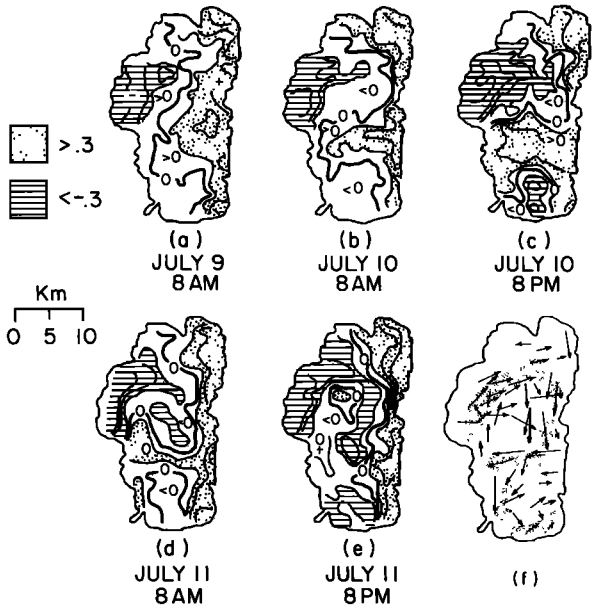

Fig. 2. (*a*)–(*e*) Surface temperature difference fields from a sequence of five images covering 60 hours in July 1980. The time and data of each image is shown. Shadings indicate temperatures 0.3°C warmer or colder than the spatial mean. The other contour levels are ±0.5°C, ±1.0°C, and ±1.5°C. (*f*) Horizontal displacements of identifiable features in the surface temperature fields derived from all pairs of images separated by 12 or 24 hours. The broad, lightly stipled arrows show the general summer circulation inferred from these displacements.

Lake Tahoe

Lake Tahoe (39°N, 120°W) is a deep, moderately large lake (501 m maximum, 313 m mean depth, 499 km^2 surface area) fitting approximately into a rectangle 20 by 30 km (Figure 1). Around most of the lake there is little shelf area, and it forms a fairly regular, nearly straight-sided basin, As such, it is more conducive to Kelvin wave dynamics [*Ou and Bennett*, 1979] than to topographic Rossby waves [*Mysak et al.*, 1983; *Mysak*, 1985], but the difference between the two is not emphasized. The scaling of the previous section suggests that the relatively flat bottom makes the barotropic component of the response more sensitive to the wind stress curl, but the extreme depth of the lake should cause the magnitude of this component to be small. The lake stratifies in spring and summer and develops a 10- to 20-m mixed layer [*Myrup et al.*, 1979]. The Rossby number for typical currents of 10–20 cm/s, as measured by *Dillon and Powell* [1976, 1979], is 0.05–0.1, and the internal deformation radius is 3–5 km for normal summer stratification. The lake is surrounded by steep mountains, and the summer winds in the basin follow a repeated diurnal cycle caused by radiation on the slopes and lake-land temperature differences. The diurnal cycle is usually dominated by winds from the southwest which reach a peak of 5–10 m/s in the afternoon and decrease after sunset.

The only estimates of Lake Tahoe's basin-wide circulation come from sequences of IR satellite images [*Strub et al.*, 1984]. Previous horizontal temperature tows [*Leigh-Abbott et al.*, 1978] and temperature sections across the lake [*Abbott et al.*, 1984; *Strub et al.*, 1984] provide evidence that the southwesterly afternoon winds cause upwelling on the west of the basin, while warmer water is accumulated and downwelled on the east. These colder and warmer water masses serve as tracers in the satellite images and allow the inference of the surface circulation. Figure 2, adapted from *Strub et al.* [1984], shows one sequence of five images, along with a composite picture of parcel displacements inferred from 60 spring and summer

TABLE 1. Numerical Model Experiments: Variation in Wind Forcing

	Wind Magnitude		Wind Direction	
Experiment	In Time	In Space	In Time	In Space
1	constant 10 /ms	constant 10 m/s	constant SSW	constant SSW
2*	variable max = 9 m/s	constant	constant SSW	constant SSW
3†	variable	constant	variable	constant
4‡	variable	variable	variable	variable

*Gaussian peak at 1400 LT.

†Winds measured hourly at one station on the NW coast, applied uniformly over the entire lake.

‡Bilinearly interpolated from measurements at seven stations around the lake.

images (1980–1982). In the five-image sequence, cold water from the upwelling region in the northwest is carried clockwise toward the northeast and then southward, while on the opposite side of the anticyclonic gyre, warm water crosses the basin to the west at midlake and continues north. Parcel trajectories taken from all pairs of images separated by 24 hours or less are shown in Figure 2*f* and indicate a strong northern anticyclonic gyre and a weaker southern cyclonic gyre. This circulation pattern differs from the single cyclonic gyre reported in the literature for other stratified basins when forced by moderate diurnal winds.

3. Methods

To clarify the dynamics responsible for the wind-driven circulation in Lake Tahoe and other stratified basins of moderate size, a numerical model was forced with a variety of wind fields. The model used is a finite difference, multilayer, hydrostatic, linear, primitive equation model. Since the emphasis is on surface transport, the present experiment uses three layers, two upper layers that are each 15 m thick at rest and a lower layer that extends to the bottom of the lake (up to 500 m). Transport in the top layer is used to examine surface circulation; vertical displacements of the internal layer surfaces are used to indicate upwelling and the propagation of long-period internal waves. The lake's bathymetry was digitized to the 1-km grid spacing used in the model. Further details of the model are presented in the appendix.

The model was driven by wind stress at the surface, calculated from wind velocity $\mathbf{U}_a$ using a bulk formula, $\tau = \rho C_D \mathbf{U}_a|\mathbf{U}_a|$ with $C_D = 1.3(10^{-3})$. Four different wind fields were used in the numerical experiments (Table 1). In experiment 1 the model was driven by a wind stress from the southwest that was constant in space and time. Next, the model was run with two kinds of time varying but horizontally uniform winds. Experiment 2 tested the effects of temporal variation in wind speed but not direction by driving the model with wind that was always from the southwest, with a diurnal maximum in midafternoon. This was the simplest approximation to the typical diurnal pattern. Experiment 3 used measured hourly winds from one well exposed location on the shore of the lake, applied uniformly over the lake's surface. This allowed temporal (but not spatial) variation of both wind speed and direction. In experiment 4 the model was driven by hourly wind fields that were constructed from bilinearly interpolated hourly averages of winds measured at seven locations around the lake's perimeter. This tested the effect of both spatial and temporal variation in wind speed and direction.

The experiments with diurnally varying winds were run for up to 12 days, repeating the wind forcing each day. Hourly averages of surface displacements and water velocities at each grid point of the model were saved and plotted. Trajectories were calculated for neutral parcels that were started at each grid point and moved by advection. Two-day residual velocities were formed from the 48-hour net dispalcements of the parcels.

4. Results

In experiment 1, where the model was driven by a constant and uniform 10 m/s southwest wind, the lake responded quickly and simply with surface drift in the direction of the wind. Upwelling occurred on the west side of the basin, especially in the northwest where the coldest water is seen in the satellite images (Figure 2). Downwelling occurred on the east and especially in the northeast. This experiment demonstrates the short-term response of the lake during idealized afternoon wind events, sweeping the lake with winds from the southwest for 3–6 hours. The results agree qualitatively with midlake observations by *Dillon and Powell* [1976, 1979], who saw a slablike response to the wind, with currents of 10–20 cm/s in the mixed layer.

In experiment 2, diurnal variability of the wind forcing was approximated with a repeated 24-hour cycle of southwest winds, beginning in the morning, peaking at ~9 m/s at 1400 LT, and stopping by late evening. The response of the lake during the initial wind event was similar to experiment 1. The surfaces of the three layers at the end of this first wind cycle

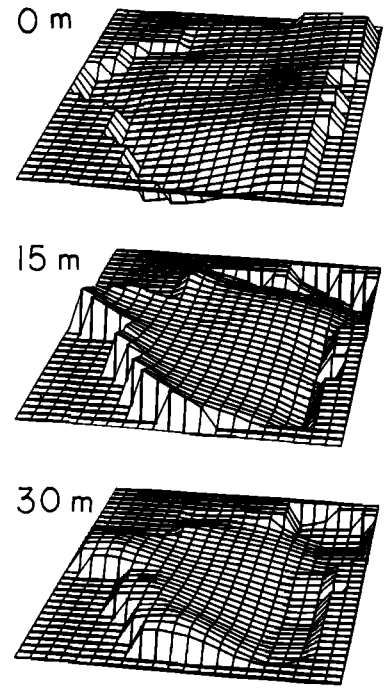

Fig. 3. Surface displacements of the three model layers in experiment 2 after the first 12-hour wind cycle. Winds are uniformly from the SSW and peak at hour 6 (1400 LT) at 9 m/s, dropping to zero by hour 14 (2200 LT). North is at the top of the figure. Displacements of the top surface (0 m) are greatly exaggerated, with maximum values of 0.5 cm. The maximum values of the vertical displacements of the interfaces at 15 m and 30 m, respectively, are approximately 8 m and 6 m. Grid points on land have zero displacements and appear flat.

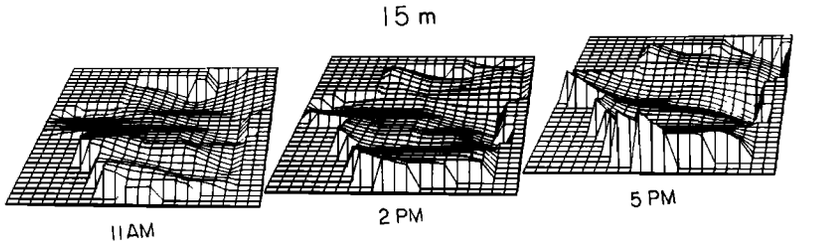

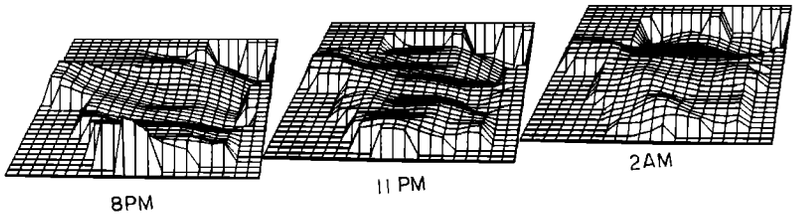

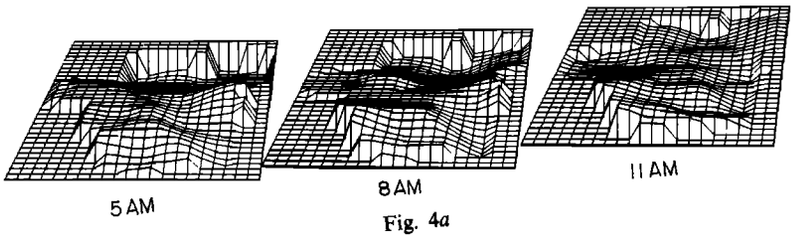

Fig. 4*a*

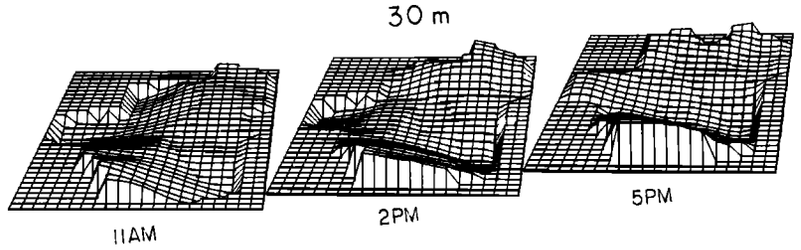

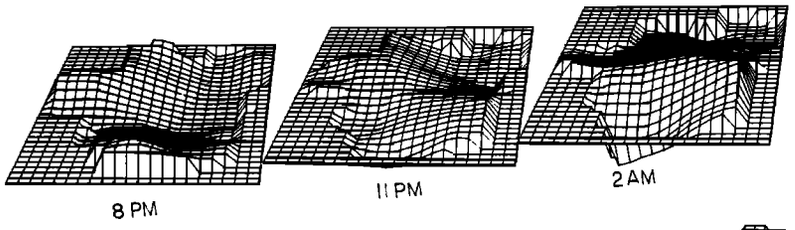

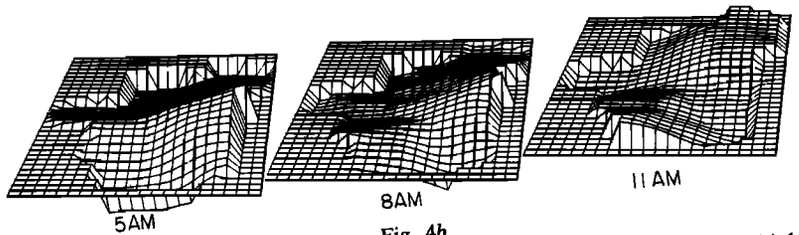

Fig. 4*b*

Fig. 4. The diurnal cycle of interface displacements during days 9 and 10 of experiment 2 at (*a*) 15 m, and (*b*) 30 m. North is toward the top of the rectangular grids. Maximum displacements are 6–8 m at both levels. Interface displacements during days 9 and 10 of experiment 4 follow a similar diurnal cycle but with reduced vertical displacements reaching maximum values of 1–2 m.

are shown in Figure 3. The top surface (0 m, greatly exaggerated) shows the setup caused by surface currents to the northeast. The second and third layer surfaces (initially, 15 and 30 m deep) show the upwelling and downwelling regions. The steeper slope of the upwelled interface nearest the top is a feature seen in analytic models with three or more layers, such as *Csanady*'s [1982] analysis of coastal upwelling. The maximum vertical displacements seen in this figure are ~0.5 cm at the top and 5–6 m at the internal interfaces. Currents at the end of the first wind cycle are with the wind at ~30 cm/s in the top layer and oppose the wind at ~5 cm/s in the second layer. Transport in the very thick bottom layer provides the rest of the return flow necessary for mass conservation.

With the relaxation of the wind the pressure gradients set

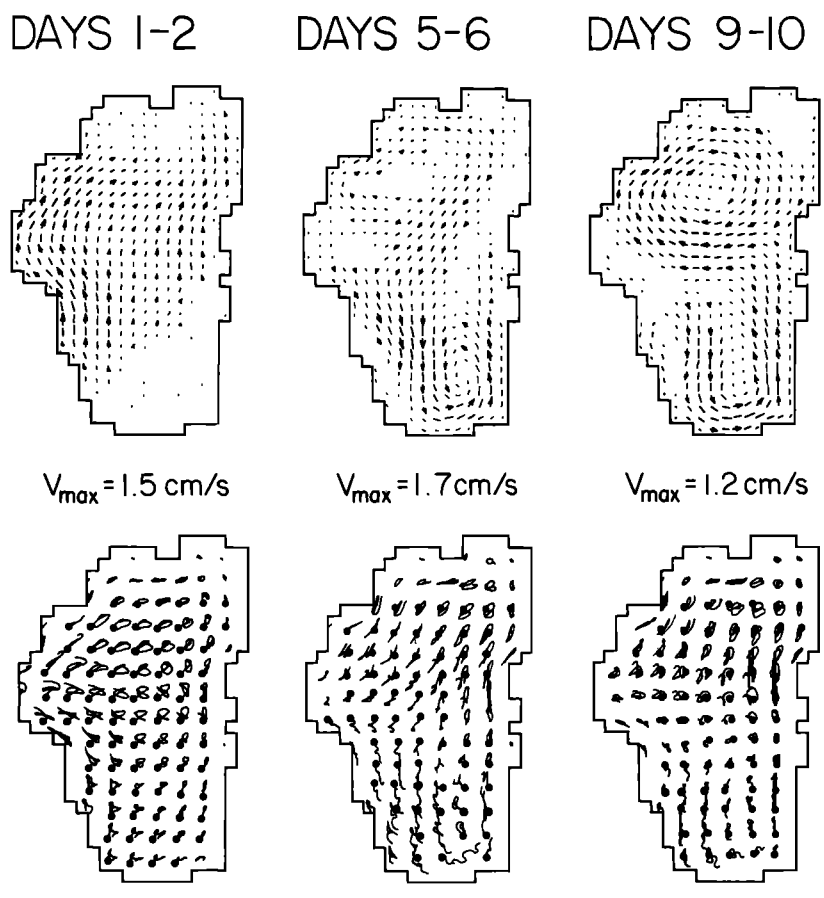

Fig. 5. Forty-eight-hour residual currents (top) and trajectories (bottom) during days 1–2, 5–6, and 9–10 of experiment 2. The residual velocities are formed by calculating the difference between the endpoints of the trajectories and dividing by the elapsed time. The maximum residual velocity of each field is depicted as a vector with length equal to the grid spacing and the value is shown beneath each field.

up by surface displacements begin to reverse the flow. The Coriolis force causes the nearshore internal displacements to stay near the coast and travel cyclonically around the lake. After a number of diurnal wind cycles, a repeated, nearly regular, diurnal response is established. Sequences of the interface displacements are seen in Figure 4 for days 9 and 10 of experiment 2. Near-surface upwelling develops on the 15-m interface each afternoon on the west and southwest coasts. The uplifted region propagates cyclonically around only a fraction of the basin circumference before the next afternoon's wind raises the interface on the west and depresses it on the east again. At 30 m the response is different. A saddle shape is seen, with two raised coastal areas caused by afternoon upwelling on alternate days. The long-wave gravity phase speed for this interface is approximately 0.45 m/s, and the period for travel around the perimeter of the lake (~80 km) is close enough to 2 days to allow a "near resonance" between the second internal mode and the diurnal winds. An approximate steady state is achieved by the end of 10–12 days.

Figure 5 shows 48-hour parcel trajectories and residual currents for experiment 2, during days 1–2, 5–6, and 9–10. The pattern which develops is that of a cyclonic gyre in the southern basin, with a weaker anticyclonic gyre in the north. Generally, the net horizontal displacement is small compared to the total trajectory length, and residual velocities are less than an order of magnitude of the instantaneous velocities. The northern anticyclonic gyre does not become established until after the sixth day of integration, while the cyclonic gyre in the south appears after the second day and grows until the sixth day, when it begins to decline slightly as the anticyclonic gyre appears.

At first glance the final residual circulation of Figure 5 resembles the mean circulation inferred from the satellite images (Figure 2). There are a number of differences, however, between the circulation seen in Figures 4 and 5 and the circulation inferred from the satellite images and past observations. The strong anticyclonic northern gyre indicated by the satellite images develops too slowly in experiment 2 (Figure 5) and is weak, whereas the cyclonic southern gyre develops rapidly and is too dominant. The simulated hourly surface currents grow to 30 or 40 cm/s, where past measurements are only 10–20 cm/s [*Dillon and Powell*, 1976, 1979]. The modeled interface displacements are 6–8 m, while observed isotherm displacements in midsummer are only 1–2 m [*Abbott et al.*, 1984]. The residual simulated velocities, on the other hand, are too weak, 1–2 cm/s, compared to the daily net velocities of 4–5 cm/s inferred from the satellite images [*Strub et al.*, 1984] and values of 5–8 cm/s found by averaging the measured velocities of *Dillon and Powell* [1979] over a 24-hour period. The instantaneous currents in the model are also qualitatively different from the measurements, fluctuating greatly in direction, while the measured currents were more continuous in direction.

To assess the impact of changing wind direction, as well as

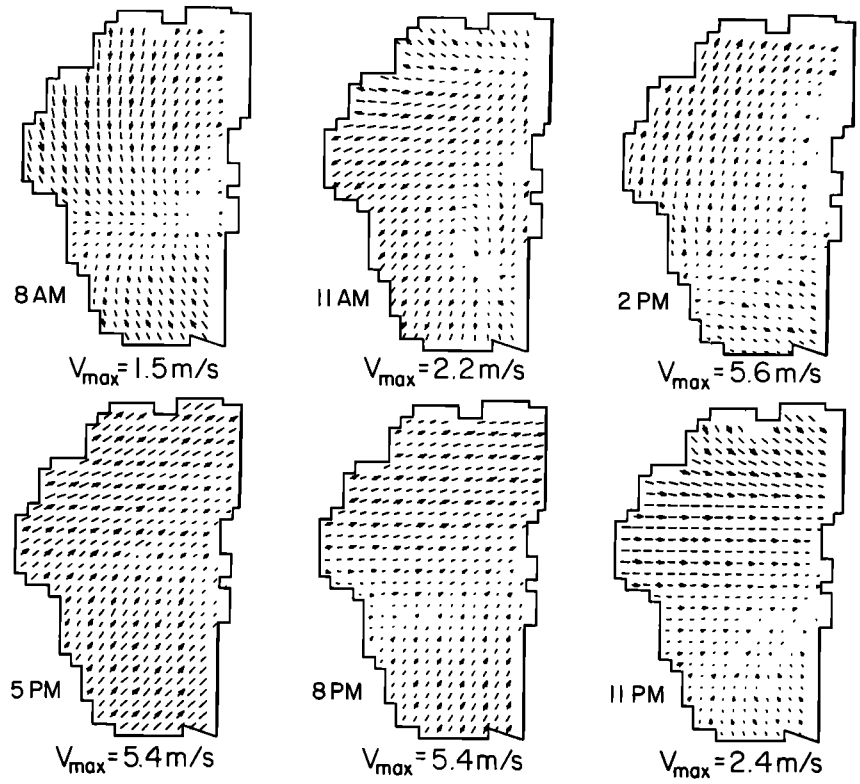

Fig. 6. Representative wind fields used to drive the lake model in experiment 4. Note the maximum hourly wind velocity indicated below each field (the scale changes in each field to allow the viewer to see the horizontal patterns of the lighter winds). The local time is indicated for each field.

speed, experiment 3 drove the model with repeated diurnal cycles of hourly averaged measured winds from one location (the northwest of the lake), applied uniformly over the lake. Wind speeds were similar to experiment 2, but the direction changed during the diurnal cycle. The strongest winds were still from the southwest and west in the afternoon. The results were nearly identical to experiment 2, showing that the measured temporal variation in the wind direction, if applied uniformly over the lake, made little difference in the response.

Experiment 4 was designed to force the model with winds that closely approximate the true wind fields. Hourly wind fields constructed from winds measured at seven locations around the lake are shown in Figure 6, for 0800, 1100, 1400, 1700, 2000, and 2300 LT on August 2, 1982. Winds on that day were typical of the diurnal summer regime, the data was complete and the clocks on all anemometers were recently synchronized. Satellite images from August 2–4, 1982, showed patterns similar to Figure 2, indicating that the wind forcing was causing the kind of lake response we seek to explain. The first panel of Figure 6 (0800 LT) shows weak, downslope, offshore night winds around most of the lake, caused by drainage of cold air in the basin and upward convection over the warmer lake. After sunrise, light upslope, onshore winds begin toward the west first and then toward nearly all shore areas by late morning. In the afternoon, solar radiation on the northeastern mountain slopes causes the strongest winds over the lake to come from the southwest, swinging to the west in the evening. An area of lighter winds across the middle of the lake divides the north and south lake into regions of anticyclonic and cyclonic wind stress, respectively. After midnight, the offshore winds and convergence over the lake seen in the 0800 LT panel is reestablished.

Trajectories and residual currents for days 1–2, 5–6, and 9–10 of experiment 4 are shown in Figure 7. The large anticyclonic gyre is established immediately in the north when the curl of the wind stress is included. The trajectories trace out nearly continuous paths around the gyre, rather than the convoluted loops of experiment 2 (Figure 5). The hourly averaged current fields for the top layer of experiment 4 (not shown) indicate that the speeds vary with a diurnal cycle, while the direction remains nearly constant. Currents at the northern side of the anticyclonic gyre are strongest in the late afternoon, reaching ~15 cm/s, while currents on the southern side of the gyre (at midlake) become strongest in the night at ~18 cm/s, representing return flow during the relaxation of the winds. Daily residual current speeds in the northern gyre are ~5 cm/s, in agreement with daily velocities inferred from the satellite images and from current measurements. Displacements of the internal surfaces have a similar diurnal cycle as those of experiment 2 (Figure 4), but are reduced to 1–2 m, also in agreement with observations. These displacements grow during the first few days and then decline, showing the essentially barotropic nature of the induced circulation. By days 9–10 the velocity fields in the second layer become similar to those in the top layer, further emphasizing that the flow is barotropic in nature. The gyres in the surface layer, driven by the curl of the wind stress, eventually communicate their vorticity downward by the curl of the friction between the top and bottom layers. A cyclonic gyre does develop in the south but is much weaker, as seen in the satellite images. Thus the inclusion of the curl of the wind stress results in much better agreement between the numerical model and past in situ measurements of currents and isotherm depths, as well as the inferred circulation from satellite images. The characteristics

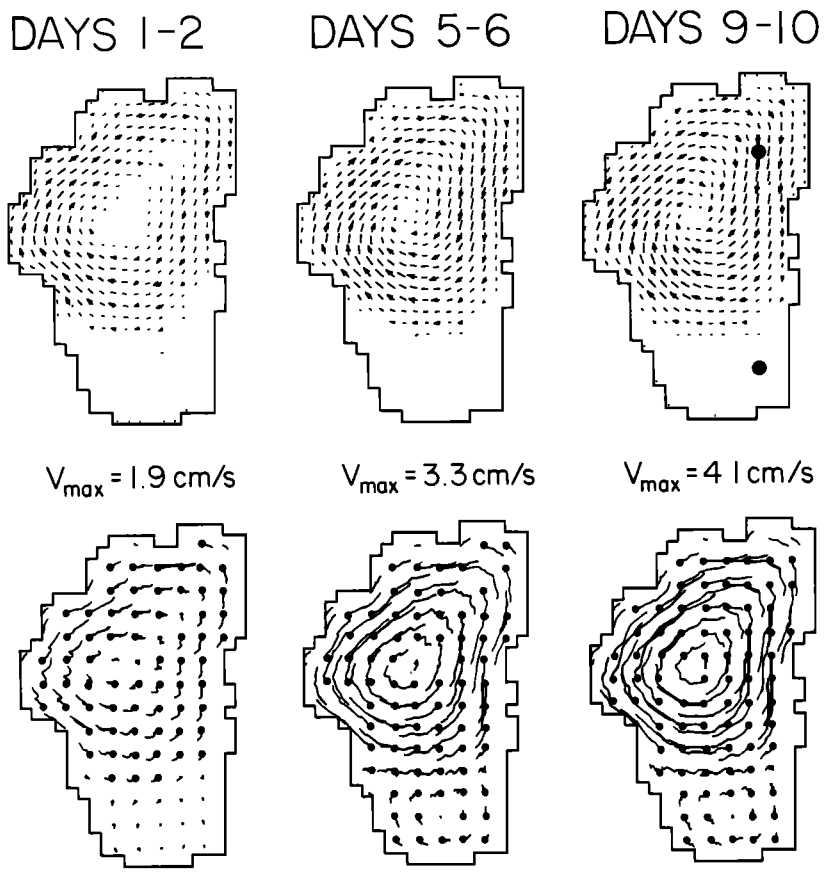

Fig. 7. Forty-eight-hour residual currents and trajectories during days 1–2, 5–6, and 9–10 of experiment 4, as in Figure 5. The two circles on the velocity field for days 9–10 show the northern and southern locations used in the vorticity analysis (Figure 8).

of this direct circulation, forced by a spatially varying wind field that includes wind stress curl, are quite different from those of the residual circulations which result from temporally varying wind fields without the spatial variations.

5. Discussion

The contrast between the inferred summer circulation at Lake Tahoe and that of other lakes in the literature is analogous to the contrast between the circulations in model experiments 4 and 2 (Figures 7 and 5). The wind stress curl drives a direct anticyclonic circulation in experiment 4 which eventually extends to the second layer. As time progresses, maximum interface displacements decline, emphasizing the barotropic nature of the response. In contrast, horizontally uniform winds in experiment 2 (and 3) produce baroclinic, oscillatory currents that change direction and magnitude over each diurnal cycle, resulting in a residual cyclonic gyre in the south. The anticyclonic gyre in the north develops only after 6 days of forcing. Instantaneous currents and interface displacements are unrealistically large, and the residual circulation is weak.

One can understand the basic difference between the two cases by dividing the water velocity into irrotational and nondivergent components, $\mathbf{v} = -\nabla\phi + \mathbf{k} \times \nabla\psi = \mathbf{v}_\phi + \mathbf{v}_\psi$, where ϕ and ψ are the velocity potential and stream function, respectively. The equations for the divergence and the vorticity are then [*Simons*, 1980]

$$\frac{\partial}{\partial t}(\text{div } \mathbf{v}_\phi) = \mathbf{k} \cdot \text{curl } (f\mathbf{v}_\psi) - \text{div}\left(\frac{H\nabla p}{\rho}\right) + \text{div } (\mathbf{F}) \qquad (3a)$$

$$\frac{\partial}{\partial t}(\mathbf{k} \cdot \text{curl } \mathbf{v}_\psi) = -f \text{ div } (\mathbf{v}_\phi) - \frac{1}{\rho} J(H, p) + \mathbf{k} \cdot \text{curl } (\mathbf{F}) \qquad (3b)$$

where $\mathbf{k} \cdot \text{curl } (\mathbf{v})$ is the vorticity of the currents (not the transport), H is the variable depth, p is the surface pressure, $\mathbf{F}$ includes the surface wind stress and other frictional and internal pressure forces, and J is the Jacobian operator. Equation (3*b*) is another form of the vorticity equations (1) and (2) presented earlier. If there is no wind stress curl in (3*b*), as in experiments 2–3, vorticity must arise through the divergent velocity, interactions between depth and pressure (caused by interface displacements), and curl of the internal frictions and pressures. Most of these terms involve divergent motions of the baroclinic modes. Large interface displacements, associated with strong, divergent baroclinic motions, must first be generated via (3*a*) and its boundary conditions before vorticity can arise as a secondary response. Energy is then slowly transferred from the velocity and pressure fields to the vorticity via (3*b*). If there is a curl of the wind stress, as in experiment 4, wind energy can be transferred directly (not as a secondary effect) to rotational currents which fit into the basin with closed streamlines, along with a reduced baroclinic response.

Attempting to further examine the balance of terms in the surface vorticity budget (2) by simple scaling proves inconclusive. The magnitudes of the first three terms on the right of (2) (the pressure term, the divergence term, and the wind stress curl) are all of the same order of magnitude, while the horizon-

tal friction and the curl of the bottom friction are much smaller. This scaling, however, applies to the peak values of oscillating terms, not to the longer averages that determine the residual currents. *Ou and Bennett* [1979] present an analysis of residual currents driven by horizontally uniform winds and describe conditions for cyclonic and anticyclonic flow. For a large, deep lake with a relatively shallow thermocline, driven by diurnally varying but horizontally uniform winds, their conclusions imply a cyclonic secondary circulation, as seen in the southern end of our model experiment 2. In lieu of an analytic theory which allows us to compare the time histories of all the terms of the vorticity budget, we have used the numerical model to calculate the terms of (2) at a number of locations in the surface layer of the lake, for experiments 2 and 4. Hourly averaged values of the total transport vorticity in the surface layer are presented in Figure 8 for experiments 2 and 4 at two locations (Figure 7), one each in the northern and southern gyres.

In the northern gyre the anticyclonic motion is arrived at in very different ways in the two experiments. The oscillatory nature of the experiment 2 surface currents is reflected in the oscillating vorticity shown in Figure 8. The two-day mean vorticity does finally become slightly anticyclonic between days 4 and 6, but the ratio of the daily mean vorticity to the peak-to-peak range of oscillation is only 0.3 by the tenth day. In experiment 4 the situation is reversed, with a mean anticyclonic circulation generated immediately, becoming greater than the range of oscillations by the end of the second day. By the tenth day the ratio of the mean value to the peak-to-peak range is 3.0, illustrating the reversal of the roles of the mean and oscillating components. Time histories of the components of the vorticity budgets (not shown) confirm the simple scale analysis result; that is, the peak values of the pressure, divergence, and wind stress curl terms are all of similar magnitudes in the two experiments. The two-day mean values, on the other hand, show an average balance in experiment 2 between the pressure term, which drives the anticyclonic vorticity, and the two friction terms, which keep the vorticity from growing further. In experiment 4 the mean balance is between the wind stress curl and the friction components, resulting in a much stronger anticyclonic flow. Thus the driving mechanism of the mean anticyclonic gyre in the northern basin is the curl of the wind stress, when present, or the pressure term otherwise. The divergence term has large peak values but oscillates with a nearly zero daily mean. The two frictional terms grow with the vorticity, opposing its continued increase and redistributing it both vertically and horizontally.

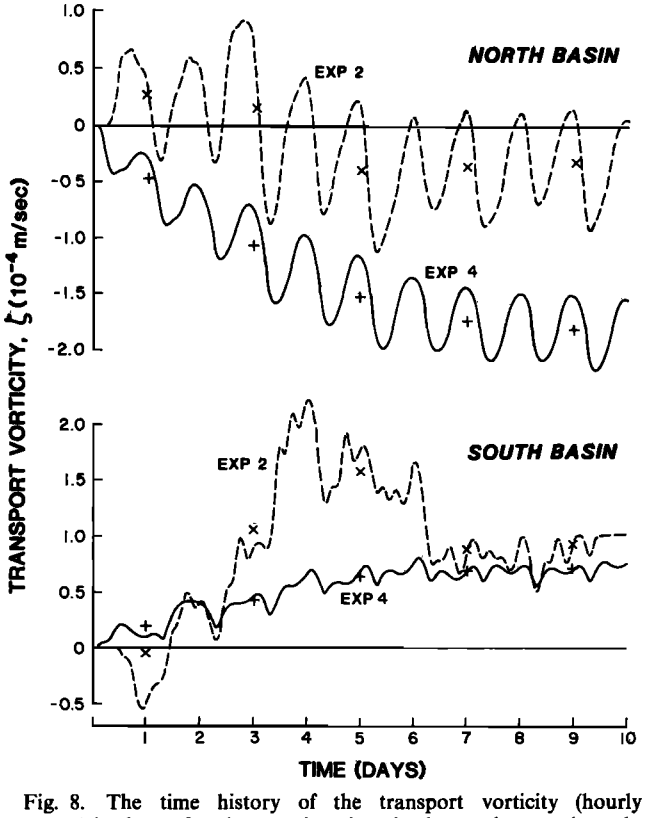

Fig. 8. The time history of the transport vorticity (hourly averages) in the surface layer at locations in the northern and southern gyres (see Figure 7). Experiment 4 (with wind stress curl) is shown by the solid curve, and experiment 2 (without wind stress curl) is shown by the dashed curve. Two-day mean values are indicated for experiments 4 (pluses) and 2 (crosses).

The picture is similar for the southern cyclonic gyre. In experiment 4 the vorticity shows a steady development of the cyclonic gyre, with small oscillations about the mean. The average balance is between the wind stress curl and the friction terms (as in the north). Without wind stress curl the vorticity fluctuates until the seventh day. The mean balance is between the pressure and friction terms (again, as in the north), finally resulting in a cyclonic circulation similar in magnitude to that established in experiment 4 by the wind stress curl.

This analysis of the vorticity budget underscores the critical importance of the wind stress curl. Yet the reported agreement between observed currents in the Great Lakes and Lake Kinneret and models of those lakes, driven by horizontally uniform winds, argues against the importance of the wind stress curl. We conclude that Lake Tahoe differs from the other basins in that the scale for the horizontal variation in the wind field is the same size as the lake; that is, the mountain basin which shapes the diurnal wind field in the summer is the same basin that forms the lake. Thus the argument that the scale of variation in the winds is much larger than the lake cannot be used. If this explanation is valid, the results should apply to a great number of moderately large lakes throughout the world in basins surrounded by complex topography (e.g., mountain basins).

The results should also apply to the coastal ocean in locations such as the west coast of the continental United States, where the winds are known to have considerable variability on the same scale as the width of the continental shelf and the internal Rossby radius of deformation [*Nelson*, 1977; *Friehe and Winant*, 1982]. Unfortunately, wind variability on these scales is difficult to measure over water and is not well known over most coastal ocean sites. Many models of the coastal ocean have neglected horizontal variations in the wind, although *Pedlosky* [1974] showed the importance of the wind stress curl in a steady state model, and *Halpern* [1976] found better correlation between the strength of the poleward undercurrent and the measured (cross-shelf) curl of the wind stress than between the undercurrent and the wind stress itself. The role of wind stress curl has been examined more recently by *Chelton* [1982], and coastal models have attempted to include a realistic curl of the wind stress in some fashion. *O'Brien and Heburn* [1983], applying the curl uniformly along the coast, included sufficient curl in their wind forcing next to the coast to match the interior Sverdrup flow (obtained from current

meter records), and *McCreary and Chao* [1985] included a constant wind stress curl, similar in magnitude to the climatological magnitude found by *Nelson* [1977] off the coast of North America. In both model studies the inclusion of the wind stress curl increased the strength of the poleward undercurrent to more realistic values. These studies demonstrate the importance of the wind stress curl in the coastal ocean but do not include the kind of mesoscale structure in the wind forcing seen by aircraft surveys made off the California coast [*Friehe and Winant*, 1982]. Realistic horizontal wind fields are probably more easily monitored over and around large lakes, as is currently being done in the Great Lakes. These basins and their coastal regions may then serve as models of the coastal ocean. Results from Lake Tahoe suggest that experiments and models of these well-monitored systems, as reported by *Schwab et al.* [1984], could increase our understanding of basin and coastal dynamics by emphasizing, rather than minimizing, the role of horizontal variations in the wind.

6. Summary and Conclusions

A numerical model has been used to determine the wind-driven circulation in a moderately large, stratified, closed basin. Three experiments were run using winds that were horizontally uniform in space and either constant or diurnally varying in time. A fourth experiment used wind forcing which varied both spatially and temporally in a realistic manner.

Two kinds of circulations resulted from the wind forcing: residual and direct. The three experiments with horizontally uniform winds produced residual circulations with large baroclinic motions, fluctuating instantaneous currents, and weak mean circulations. The net displacements of water parcels at the end of each diurnal cycle were small compared to their total trajectory length (Figure 5). The fourth experiment included measured horizontal variation of the dirunal wind fields and resulted in a direct circulation, with a stronger mean circulation (Figure 7) and greatly reduced current fluctuations and baroclinic motions. The final two-day mean circulations (the vectors from days 9–10 in Figures 5 and 7) caused by both kinds of wind forcing appear qualitatively (but not quantitatively) similar to each other and similar to the double gyre inferred from satellite imagery (Figure 2). If only horizontally uniform winds had been used in the model, we might have concluded that the observed circulation was a result of large baroclinic "vorticity waves," as in the Great Lakes, and that this circulation took a week of repeated diurnal winds to develop. This would still have left discrepancies with past current measurements that lacked the fluctuations in direction seen in the trajectories in Figure 5 and had weaker instantaneous velocities and stronger mean velocities. The great magnitudes of the vertical displacements of the internal interfaces would also have different from past measurements. The direct circulation forced by the horizontally varying winds removes these discrepancies.

Examination of the modeled vorticity budget in the surface layer clearly demonstrates the role of the wind stress curl in rapidly creating the direct, two-gyre circulation. In its absence, wind energy must first create large divergent motions, internal interface displacements, and associated pressure gradients before the vorticity of the lake-wide gyres can be created. Stated differently, the kinetic energy input by the wind must first be transformed to available potential energy in the raised internal density surfaces and then transformed further into the kinetic energy associated with the basin gyres. The presence of the wind stress curl allows a much more efficient transfer of the wind's kinetic energy directly into the gyral circulation patterns.

Lake Tahoe's double gyre, dominated by the large, anticyclonic northern gyre, contrasts with the single cyclonic gyre reported for other stratified basins. We suggest that the difference results from the fact that the scale of wind variation in Lake Tahoe is the same as the horizontal lake dimension, since both are created by the same mountain basin. If so, the results should apply to other moderately large lakes in basins of varied terrain. The results also apply to regions of the coastal ocean where the variation in the wind stress occurs over the same spatial scales as the width of the shelf.

Appendix: The Numerical Model

The numerical model used incorporates a multilayer vertical structure [*Cheng et al.*, 1976; *Simons*, 1980] shown in Figure A1. Each layer has a constant density. Layer surfaces are free to move in the vertical in response to the mass redistribution in the layers, but no mass is exchanged between layers. The model is expressed in terms of the integrated transports U_k and V_k in the kth layer, defined as

$$U_k = \int u_k\, dz = u_k\, d_k \qquad V_k = \int v_k\, dz = v_k\, d_k \tag{A1}$$

where u_k, v_k are the x and y velocities in the kth layer, d_k is the instantaneous thickness of the kth layer, $d_k = (h_k - h_{k+1} + \eta_k - \eta_{k+1})$, h_k is the resting height of the layer, and η_k is the vertical displacement of the layer from its resting height. When the linear equations for the conservation of momentum are integrated over each layer, the resulting model equations for the transports become

$$\begin{aligned}\frac{\partial U_k}{\partial t} &= -\frac{d_k}{\rho_k}\frac{\partial p_k}{\partial x} + fV_k - A_h\nabla^2 U_k + \frac{1}{\rho}(\tau_{xk} - \tau_{bxk}) \\ \frac{\partial V_k}{\partial t} &= -\frac{d_k}{\rho_k}\frac{\partial p_k}{\partial y} - fU_k - A_h\nabla^2 V_k + \frac{1}{\rho}(\tau_{yk} - \tau_{byk})\end{aligned} \tag{A2}$$

where p_k is pressure at the top of the layer, ρ_k is the layer density, f is the Coriolis parameter, τ_{xk} and τ_{yk} are the interfacial momentum stresses on the upper surface of the layer in the x and y directions, and τ_{bxk} and τ_{byk} are the corresponding stresses on the lower surface of the layer.

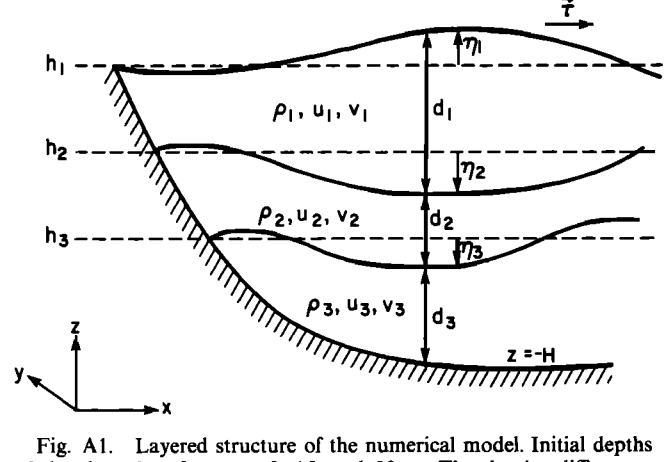

Fig. A1. Layered structure of the numerical model. Initial depths of the three interfaces are 0, 15, and 30 m. The density differences between internal layers are both 0.4 kg m^{-3}.

The fluid is assumed incompressible, reducing the conservation of mass to the continuity equation. This is integrated from the bottom up to a layer surface to find the vertical velocity, which is then used to find the change in height of each surface:

$$\Delta\eta_k = -\Delta t \sum_{i=L}^{k} \left(\frac{\partial U}{\partial x} + \frac{\partial V}{\partial y}\right)_i$$
$$\eta_k(t) = \eta_k(t - \Delta t) + \Delta\eta_k \qquad \text{(A3)}$$

where L is the bottom layer number and Δt is the time step used. Equations (A2) and (A3) form three equations in the three unknowns U, V, and η. The lateral boundary conditions are that no flow is allowed normal to the boundary. The wind stress at the surface of the lake and the bottom stress are described below.

The three variables are discretized on a single staggered grid system shown in Figure A2, which allows simple centered differences for the horizontal gradients of η; other quantities must be averaged to find a value at a location of one of the other variables. In general, the grid does well for geophysical fluid motions with length scales greater than several grid spacings [*Messinger and Arakawa*, 1976; *Simons*, 1980; *Hsieh et al.*, 1983].

The pressure is evaluated from the hydrostatic relation $\partial p/\partial z = -\rho g$. The pressure gradients for the kth layer are found by summing over all layers from the kth to the surface:

$$\frac{d_k}{\rho_k}\frac{\partial p_k}{\partial x} = \frac{g d_k}{\rho_k}\sum_{i=1}^{k}(\rho_i - \rho_{i-1})\frac{\partial \eta_i}{\partial x}$$
$$\frac{d_k}{\rho_k}\frac{\partial p_k}{\partial y} = \frac{g d_k}{\rho_k}\sum_{i=1}^{k}(\rho_i - \rho_{i-1})\frac{\partial \eta_i}{\partial y} \qquad \text{(A4)}$$

where g is the acceleration of gravity. At the surface (layer 1) the density of air is taken to be zero. A constant value of 10^{-4} s^{-1} is used for f, and the value of A_h is constant at 10 m^2 s^{-1}. The stresses on the layer surfaces are either the wind stress, bottom stress, or interfacial stresses. Wind stress at the surface is calculated from wind velocities using a bulk formula, $\tau = \rho_a C_D \mathbf{U}_a|\mathbf{U}_a|$, with ρ_a the air density set constant at 1.0 kg m^{-3} at Lake Tahoe's altitude, C_D taken constant at $1.3(10^{-3})$, and the wind velocity $\mathbf{U}_a$ specified as stated in the text. Friction at the bottom of the lake is found with a similar quadratic drag law, $\tau_b = \rho B\mathbf{v}|\mathbf{v}|$, where B is a constant equal to $2.5(10^{-3})$, and $\mathbf{v}$ is the water velocity in the bottom layer. Interfacial stress, at the top or bottom of an internal layer, is found using a vertical eddy viscosity, $\tau = \rho A_v(\partial v/\partial z)$, where $\mathbf{v}$ is water velocity, not transport. The finite difference is found over Δz, the vertical distance between the midpoints of the two layers, and A_v is the vertical eddy viscosity, set equal to $5(10^{-4})$ m^2 s^{-1}.

An explicit forward time step of 10 s is used to increment U and V using (A2) and (A4). The vertical displacements are then incremented using (A3).

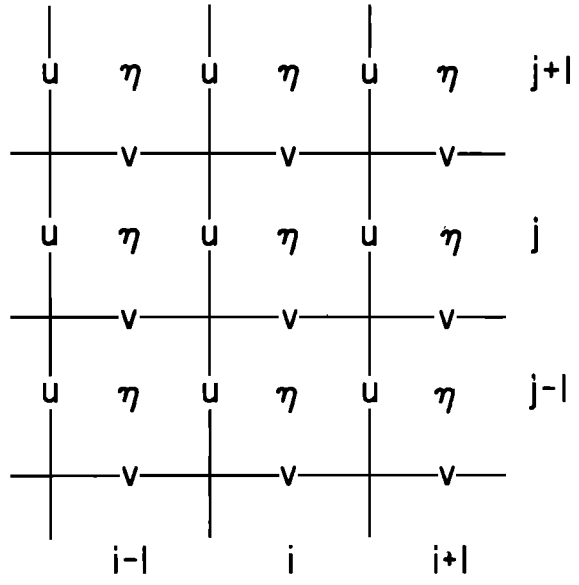

Fig. A2. Horizontal grid structure of the numerical model. U and V are transports in the x and y directions; η is the interface displacement. Grid spacing is approximately 1 km in both directions.

Acknowledgments. Funding for this work was provided by NASA grant NAG5-217. Discussions with M. R. Abbott were helpful, as was his collaboration on the satellite and field data analysis reported elsewhere. The numerical model was adapted from an earlier model formulated by T. M. Dillon. The review of D. Schwab provided valuable insight into the relative importance of wind stress curl and variations of depth for the barotropic case. Computer time to run the model was made available by the National Center for Atmospheric Research (NCAR), which is funded by the National Science Foundation. Access to NCAR was accomplished through facilities supplied by B. C. Weare and U. C. Davis. We would like to thank Carol Barnes and Sharon Lynch, who helped prepare an initial version of this manuscript.

REFERENCES

Abbott, M. R., K. L. Denman, T. M. Powell, P. J. Richerson, R. C. Richards, and C. R. Goldman, Mixing and the dynamics of the deep chlorophyll maximum in Lake Tahoe, *Limnol. Oceanogr.*, *29*, 862–878, 1984.

Ball, F. K., Second class motions of a shallow liquid, *J. Fluid Mech.*, *23*, 545–561, 1965.

Bennett, J. R., A three-dimensional model of Lake Ontario's summer circulation, I, Comparison with observations, *J. Phys. Oceanogr.*, *7*, 591–601, 1977.

Bennett, J. R., A three-dimensional model of Lake Ontario's summer circulation, II, A diagnostic study, *J. Phys. Oceanogr.*, *8*, 1095–1103, 1978.

Chelton, D. B., Large-scale response of the California Current to forcing by the wind stress curl, *Calif. Coop. Oceanic Fish., Invest. Rep.*, *23*, pp. 130–148, 1982.

Cheng, R. T., and V. Casulli, On Lagrangian residual currents with applications in south San Francisco Bay, California, *Water Resour. Res.*, *18*, 1652–1662, 1982.

Cheng, R. T., T. M. Powell, and T. M. Dillon, Numerical models of wind-driven circulation in lakes, *Appl. Math. Modeling*, *1*, 141–159, 1976.

Csanady, G. T., Hydrodynamics of large lakes, *Annu. Rev. Fluid Mech.*, *7*, 357–386, 1975.

Csanady, G. T., On the structure of transient upwelling events, *J. Phys. Oceanogr.*, *12*, 84–96, 1982.

Dillon, T. M., and T. M. Powell, Low-frequency turbulence spectra in the mixed layer of Lake Tahoe, California-Nevada, *J. Geophys. Res.*, *81*, 6421–6427, 1976.

Dillon, T. M., and T. M. Powell, Observations of a surface mixed layer, *Deep Sea Res.*, *26A*, 915–932, 1979.

Emery, K. O., and G. T. Csanady, Surface circulation of lakes and nearly land-locked seas, *Proc. U.S. Natl. Acad. Sci.*, *70*, 93–97, 1973.

Friehe, C. A., and C. D. Winant, Observations of wind and sea surface temperature structure off the northern California coast, paper presented at First International Conference on Meteorology and Air/Sea Interaction of the Coastal Zone, Am. Meteorol. Soc., The Hague, 1982.

Goldman, C. R., Eutrophication of Lake Tahoe emphasizing water quality, *Rep. EPA-660/3-74-034*, 408 pp., U.S. Govt. Print. Off., Washington, D. C., 1974.

Halpern, D., Measurements of near-surface wind stress over an upwelling region near the Oregon coast, *J. Phys. Oceanogr.*, *6*, 108–112, 1976.

Hsieh, W. W., M. K. Davey, and R. C. Wajsowicz, The free Kelvin wave in finite-difference numerical models, *J. Phys. Oceanogr., 13*, 1383–1397, 1983.

Huang, J. C. K., and J. H. Saylor, Vorticity waves in a shallow basin, *Dyn. Atmos. Oceans, 6*, 177–196, 1982.

Huang, J. C. K., and P. W. Sloss, Simulation and verification of Lake Ontario's mean state, *J. Phys. Oceanogr., 11*, 1548–1566, 1981.

Leigh-Abbott, M. R., J. A. Coil, T. M. Powell, and P. J. Richerson, Effects of a coastal front on the distribution of chlorophyll in Lake Tahoe, California-Nevada, *J. Geophys. Res., 83*, 4668–4672, 1978.

McCreary, J. P., and S. Chao, Three-dimensional shelf circulation along an eastern ocean boundary, *J. Mar. Res., 43*, 13–36, 1985.

Messinger, F., and A. Arakawa, Numerical methods used in atmospheric models, *GARP Publ. Ser., 17*(I), 64 pp., 1976.

Myrup, L. O., T. M. Powell, D. A. Godden, and C. R. Goldman, Climatological estimate of the average monthly energy and water budgets of Lake Tahoe, California-Nevada, *Water Resour. Res., 15*(6), 1499–1508, 1979.

Mysak, L. A., Elliptical topographic waves, *Geophys. Astrophys. Fluid Dyn., 31*, 93–135, 1985.

Mysak, L. A., G. Salvade, K. Hutter, and T. Scheiwiller, Lake of Lugano and topographic waves, *Nature, 306*(3), 46–48, 1983.

Nelson, C. S., Wind stress and wind stress curl over the California Current, *NOAA Tech. Rep., NMFS SSRF-714*, 87 pp., 1977.

O'Brien, J. J., and G. W. Heburn, The state-of-the-art in coastal ocean modelling: A numerical model of coastal upwelling off Peru—Including mixed layer dynamics, in *Coastal Oceanography*, edited by H. Gade, A. Edwards, and H. Svendsen, pp., 113–164, Plenum, New York, 1983.

Ou, H. W., and J. R. Bennett, A theory of the mean flow driven by long internal waves in a rotating basin, with application of Lake Kinneret, *J. Phys. Oceanogr., 9*, 1112–1125, 1979.

Pedlosky, J., Longshore currents, upwelling and bottom topography, *J. Phys. Oceanogr., 4*, 214–226, 1974.

Pickett, R. L., and F. P. Richards, Lake Ontario mean temperature and currents in July, 1972, *J. Phys. Oceanogr., 5*, 755–781, 1975.

Rao, D. B., and T. S. Murthy, Calculation of the steady state wind-driven circulation in Lake Ontario, *Arch. Meteorol. Geophys. Bioklimatol., Ser. A, 19*, 195–210, 1970.

Saylor, J. H., J. C. K. Huang, and R. O. Reid, Vortex modes in southern Lake Michigan, *J. Phys. Oceanogr., 10*, 1814–1823, 1980.

Schwab, D. J., Numerical simulation of low-frequency current fluctuations in Lake Michigan, *J. Phys. Oceanogr., 13*, 2213–2224, 1983.

Schwab, D. J., G. A. Meadows, J. R. Bennett, H. Schultz, P. C. Liu, J. E. Campbell, and H. H. Dannelongue, The response of the coastal boundary layer to wind and waves: Analysis of an experiment in Lake Erie, *J. Geophys. Res., 89*, 8043–8053, 1984.

Serruya, S., Wind, water temperature and motions in Lake Kinneret: General pattern, *Verh. Int. Ver. Theor. Angew. Limnol., 19*, 73–87, 1975.

Simons, T. J., Verification of numerical models of Lake Ontario, part II, Stratified circulations and temperature changes, *J. Phys. Oceanogr., 5*, 98–110, 1975.

Simons, T. J., Circulation models of lakes and inland seas, *Can. Bull. Fish. Aquatic Sci., 203*, 146 pp., 1980.

Simons, T. J., Reliability of circulation models, *J. Phys. Oceanogr., 15*, 1191–1204, 1985.

Strub, T., T. M. Powell, and M. R. Abbott, Temperature and transport patterns in Lake Tahoe: Satellite imagery, field data and a dynamical model, *Verh. Int. Ver. Theor. Angew. Limnol., 22*, 112–118, 1984.

T. M. Powell, Division of Environmental Studies, University of California, Davis, CA 95616.

P. T. Strub, College of Oceanography, Oregon State University, Corvallis, OR 97331.

(Received November 25, 1985;
accepted December 31, 1985.)